

Multimode space-vector overmodulation technique for enhancing voltage transfer ratio in matrix converters

Quoc-Hoan Tran^{1*}, Huu-Cong Vu², Huu-Nhan Nguyen³

¹Faculty of Standards, Metrology and Quality, Tran Dai Nghia University, Ho Chi Minh City, Vietnam

²Department of Electrical Engineering, Hanoi University of Civil Engineering, Hanoi, Vietnam

³LS Automotive Technologies Company, Gyeonggi-do 14067, Korea

*Corresponding author E-mail: hoantq@tdnu.edu.vn

Abstract

The control method of three-phase matrix converters (MCs) inherently limits the voltage transfer ratio (VTR) to 0.866 in the linear modulation region, which constrains the broader application of MCs. This paper presents a detailed investigation into a space-vector overmodulation technique aimed at enhancing the VTR of MCs. The proposed method integrates the principles of inscribed circle and hexagon vectors, as well as hexagon and basic vectors, to extend the modulation range. Explicit equations for calculating the duty ratios of active and zero vectors are derived to achieve improved VTR. The effectiveness of the approach is validated through simulation results, demonstrating accurate output voltage fundamental components.

Keywords: Matrix converter; Multimode modulation; Overmodulation; Space-vector modulation; Voltage transfer ratio.

Symbols

Symbols	Units	Description
\vec{v}_i, \vec{v}_o	V	input/output voltage vector
\vec{i}_i, \vec{i}_o	A	input/output current vector
d		duty cycle
q		voltage transfer ratio

Abbreviations

MC	Matrix Converter
VTR	Voltage Transfer Ratio
SVM	Space-Vector Modulation
ISVM	Indirect Space-Vector Modulation
DSVM	Direct Space-Vector Modulation
EMI	Electromagnetic Interference

1. Introduction

Matrix converters (MCs) have recently attracted considerable interest owing to their benefits over standard back-to-back converters, such as bidirectional power flow, sinusoidal input and output waveforms, regulated input power factor, and extended operating lifespan [1], [2]. The lack of substantial energy storage elements, like capacitors, further augments the MC's compactness, robustness, and reliability [3]. Current research on MCs primarily focuses on areas such as input filter design, commutation strategies, stabilization analysis, and modulation techniques [4].

Several types of modulation approaches with distinct characteristics have been developed to address issues in MCs, such as unbalanced input voltages, reduction of common-mode voltage, fault tolerance, and improving input/output performance [5]-[12]. However, most of these approaches limit the voltage transfer ratio (VTR) to 0.866, constraining

the broader application of MCs. To overcome this limitation, two main solutions have been explored: 1) incorporating auxiliary hardware, and 2) applying overmodulation methods. The first solution involves introducing various topologies that enhance the VTR by integrating boost circuits into the MC configuration. While effective, these topologies typically require additional passive components or switching devices, leading to increased complexity, higher losses, and larger overall system size [13]-[17]. In contrast, the second solution, which leverages overmodulation methods, is more appealing as it improves the VTR without necessitating additional hardware, thus offering a cost-effective approach [18].

In recent years, various modulation techniques have been developed to enhance the VTR of MCs. One notable approach is an overmodulation method based on predictive control, which increases the VTR to 0.987 through an automatic adjustment mechanism [15]. In the interest of space-vector modulation (SVM), an indirect overmodulation strategy has been introduced, incorporating multiple weighted vectors - namely, the inscribed circle vector, hexagon vector, and basic vector - within the indirect SVM framework [4]. Additionally, indirect space-vector overmodulation algorithms have been applied to ultrasparse MCs, improving the fundamental VTR by modifying the modulation methods in both the rectifier and inverter stages [16], [17].

Another approach involves direct SVM, where an overmodulation algorithm boosts the VTR by scaling the duty cycles of active vectors, ensuring their sum remains limited to unity [18]. This method successfully eliminates negative duty cycles for zero vectors. However, it lacks achieving the exact fundamental output voltage and imposes a significant computational burden.

To improve the VTR for MCs, an alternative space-vector overmodulation technique is presented in this study. The method considers the basic, hexagonal, and inscribed circle vectors' fundamental amplitudes. The overmodulation area is

separated into two separate sections: region I uses the inscribed circle and hexagon vectors to synthesize the output voltage vector, while region II uses the hexagon and basic vectors. The basic and hexagonal vectors' fundamental output voltage amplitudes are thoroughly examined. Finally, simulation results are shown to validate the precision and effectiveness of the proposed overmodulation technique.

2. Conventional SVM Method

As shown in Figure 1, nine bidirectional switches that enable any output phase to link with any input phase make up a three-phase MC. A low-pass filter is required to smooth the input currents to satisfy electromagnetic interference (EMI) criteria at the input. The switching states of MCs need to follow two important guidelines to function reliably: i) no input short circuit, and ii) no output open circuit.

As indicated in Table 1, the three-phase MC has 27 potential switching states because of these limitations, which are divided into three groups: there are three zero-vector states in Group II, six rotating-vector states in Group III, and eighteen active-vector states in Group I.

The following equations and the accompanying symbols in Figure 1 define the space vectors for the input/output voltages and currents:

$$\vec{v}_i = 2(v_{ia} + v_{ib}e^{j2\pi/3} + v_{ic}e^{j4\pi/3}) / 3 = V_i e^{j\alpha_i} \quad (1)$$

$$\vec{v}_o = 2(v_A + v_B e^{j2\pi/3} + v_C e^{j4\pi/3}) / 3 = V_o e^{j\alpha_o} \quad (2)$$

$$\vec{i}_i = 2(i_{ia} + i_{ib}e^{j2\pi/3} + i_{ic}e^{j4\pi/3}) / 3 = I_i e^{j\beta_i} \quad (3)$$

$$\vec{i}_o = 2(i_A + i_B e^{j2\pi/3} + i_C e^{j4\pi/3}) / 3 = I_o e^{j\beta_o} \quad (4)$$

Since their angular locations are not fixed, the rotating-vector states in Group III are typically not employed to operate the MC, which makes it challenging to create a repeating switching pattern [2]. Four active vectors are chosen from Group I to synthesize the reference output voltage vector in the standard SVM approach, while keeping the input power factor constraint at unity [7], [12]. After then, the zero vectors are used to finish the sample period.

For example, as seen in Figure 2(a) and (b), active-vector states from $\pm 1, \pm 2, \pm 3,$ and $\pm 7, \pm 8, \pm 9$ are chosen to produce the correct output voltage vector when both the input current vector and the output voltage vector fall in sector 1. The current vector is simultaneously created using active-vector

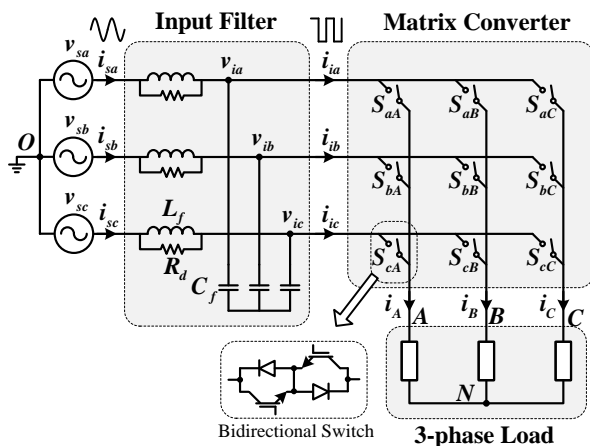


Figure 1: A common three-phase to three-phase MC configuration.

Table 1: Potential Matrix Converter Switching States

	Switching State			Output Voltage		Input Current		
	No	A	B	C	V_o	α_o	I_i	β_i
Group I	+1	a	b	b	$2v_{ab}/3$	0	$2i_A/\sqrt{3}$	$-\pi/6$
	-1	b	a	a	$-2v_{ab}/3$	0	$-2i_A/\sqrt{3}$	$-\pi/6$
	+2	b	c	c	$2v_{bc}/3$	0	$2i_B/\sqrt{3}$	$\pi/2$
	-2	c	b	b	$-2v_{bc}/3$	0	$-2i_B/\sqrt{3}$	$\pi/2$
	+3	c	a	a	$2v_{ca}/3$	0	$2i_C/\sqrt{3}$	$7\pi/6$
	-3	a	c	c	$-2v_{ca}/3$	0	$-2i_C/\sqrt{3}$	$7\pi/6$
	+4	b	a	b	$2v_{ab}/3$	$2\pi/3$	$2i_B/\sqrt{3}$	$-\pi/6$
	-4	a	b	a	$-2v_{ab}/3$	$2\pi/3$	$-2i_B/\sqrt{3}$	$-\pi/6$
	+5	c	b	c	$2v_{bc}/3$	$2\pi/3$	$2i_C/\sqrt{3}$	$\pi/2$
-5	b	c	b	$-2v_{bc}/3$	$2\pi/3$	$-2i_C/\sqrt{3}$	$\pi/2$	
+6	a	c	a	$2v_{ca}/3$	$2\pi/3$	$2i_A/\sqrt{3}$	$7\pi/6$	
-6	c	a	c	$-2v_{ca}/3$	$2\pi/3$	$-2i_A/\sqrt{3}$	$7\pi/6$	
+7	b	b	a	$2v_{ab}/3$	$4\pi/3$	$2i_C/\sqrt{3}$	$-\pi/6$	
-7	a	a	b	$-2v_{ab}/3$	$4\pi/3$	$-2i_C/\sqrt{3}$	$-\pi/6$	
+8	c	c	b	$2v_{bc}/3$	$4\pi/3$	$2i_A/\sqrt{3}$	$\pi/2$	
-8	b	b	c	$-2v_{bc}/3$	$4\pi/3$	$-2i_A/\sqrt{3}$	$\pi/2$	
+9	a	a	c	$2v_{ca}/3$	$4\pi/3$	$2i_B/\sqrt{3}$	$7\pi/6$	
-9	c	c	a	$-2v_{ca}/3$	$4\pi/3$	$-2i_B/\sqrt{3}$	$7\pi/6$	
Group II	0a	a	a	a	0	x	0	x
	0b	b	b	b	0	x	0	x
	0c	c	c	c	0	x	0	x
Group III	r1	a	b	c	V_i	α_i	I_o	β_o
	r2	a	c	b	V_i	$-\alpha_i$	I_o	$-\beta_o$
	r3	c	a	b	V_i	$2\pi/3 + \alpha_i$	I_o	$-2\pi/3 + \beta_o$
	r4	b	a	c	V_i	$2\pi/3 - \alpha_i$	I_o	$2\pi/3 - \beta_o$
	r5	b	c	a	V_i	$-2\pi/3 + \alpha_i$	I_o	$2\pi/3 + \beta_o$
	r6	c	b	a	V_i	$-2\pi/3 - \alpha_i$	I_o	$-2\pi/3 - \beta_o$

states from $\pm 1, \pm 4, \pm 7,$ and $\pm 3, \pm 6, \pm 9$. Four typical states with the two largest voltage magnitudes are selected from among these. The two largest input line-to-line voltages are v_{ab} and v_{ac} , as shown in Figure 3, when the input current vector is in sector 1. The four active-vector states ($+1, -3, -7,$ and $+9$) are chosen to produce the input current vector \vec{i}_i and the output voltage vector \vec{v}_o , according to Table 1.

A similar analysis can be applied to all combinations of output voltage and input current sectors, with the selected active-vector states summarized in Table 2. The general expression for the duty cycles is as follows:

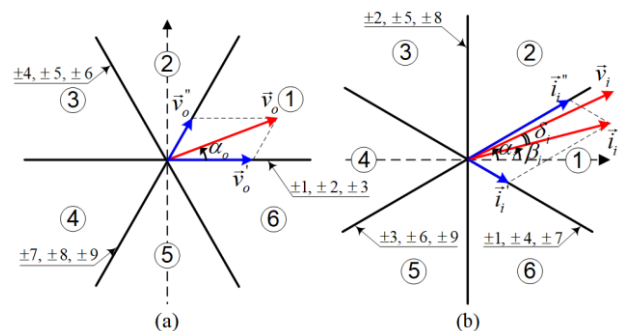


Figure 2: The location of (a) output voltage vector (b) input current vector.

$$\begin{cases} d_1 = \frac{2q}{\sqrt{3}} \frac{\sin \tilde{\alpha}_o \sin(\pi/6 - \tilde{\beta}_i)}{\cos \delta_i} \\ d_2 = \frac{2q}{\sqrt{3}} \frac{\sin \tilde{\alpha}_o \sin(\pi/6 + \tilde{\beta}_i)}{\cos \delta_i} \\ d_3 = \frac{2q}{\sqrt{3}} \frac{\sin(\pi/3 - \tilde{\alpha}_o) \sin(\pi/6 - \tilde{\beta}_i)}{\cos \delta_i} \\ d_4 = \frac{2q}{\sqrt{3}} \frac{\sin(\pi/3 - \tilde{\alpha}_o) \sin(\pi/6 + \tilde{\beta}_i)}{\cos \delta_i} \end{cases} \quad (1)$$

where $q = V_o / V_i$ is the VTR, $\delta_i = \alpha_i - \beta_i$ is the input current displacement angle, $\tilde{\alpha}_o$ and $\tilde{\beta}_i$ are defined as

$$\tilde{\alpha}_o = \alpha_o - (k_v - 1) \times \pi / 3 \quad (5)$$

$$\tilde{\beta}_i = \beta_i - (k_i - 1) \times \pi / 3 \quad (6)$$

where k_v and k_i are the output voltage sector and the input current sector, respectively.

The sample period is then concluded by applying zero space vectors, with the associated duty cycle provided by:

$$d_0 = 1 - \frac{2q}{\sqrt{3}} \frac{\cos(\pi/6 - \tilde{\alpha}_o) \cos \tilde{\beta}_i}{\cos \delta_i} \quad (7)$$

The example depicted in Figure 2, where both the input and output vectors are in sector 1, is represented by the switching pattern in Figure 4.

All duty cycles in the traditional SVM approach must meet the following requirements:

$$0 \leq d_n \leq 1; \quad n = 0, \dots, 4 \quad (8)$$

The recognized VTR limit for MCs is derived from this condition and is written as:

$$q \leq \frac{\sqrt{3}}{2} \cos \delta_i \quad (9)$$

The output voltage remains linear within this VTR range.

3. Space-Vector Overmodulation Method

As seen in (7), the duty cycle of zero vectors must be non-negative, hence the highest possible VTR is:

$$q_{\max} = \frac{\sqrt{3}}{2} \frac{\cos \delta_i}{\cos(\pi/6 - \tilde{\alpha}_o) \cos \tilde{\beta}_i} \quad (10)$$

The maximum VTR is determined by $\tilde{\alpha}_o$ and $\tilde{\beta}_i$ based on (10). Figure 5 displays the maximum VTR as a function of $\tilde{\alpha}_o$ and $\tilde{\beta}_i$, assuming a unity input power factor ($\cos \delta_i = 1$). It is evident that the maximum value of VTR is always lower than $\sqrt{3}/2$ for any values of $\tilde{\alpha}_o$ and $\tilde{\beta}_i$, as indicated by the inscribed circle vector in Figure 6.

To eliminate the dependence of the maximum VTR on the input phase angle, the maximum VTR is constrained to:

$$q_{\max} \leq \frac{\sqrt{3}}{2} \frac{\cos \delta_i}{\cos(\pi/6 - \tilde{\alpha}_o)} \quad (11)$$

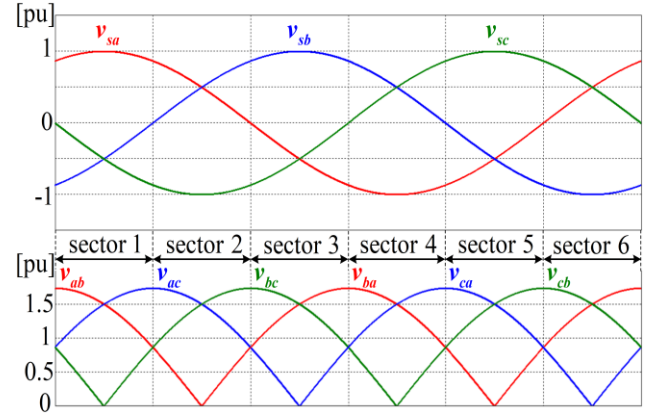


Figure 3: Input line voltages and input phase at the input power source.

This ensures that the maximum VTR q_{\max} can always reach the value of $\frac{\sqrt{3}}{2} \frac{\cos \delta_i}{\cos(\pi/6 - \tilde{\alpha}_o)}$, regardless of the value $\tilde{\beta}_i$.

Figure 6 shows the relationship between q_{\max} and $\tilde{\alpha}_o$ in (11). As is evident, the maximum VTR q_{\max} boundary takes the shape of a hexagon, and the output voltage vector can rotate along its borders for any value $\tilde{\beta}_i$. Combining the principles of the inscribed circle vector \vec{v}_{\sin} and the hexagon vector \vec{v}_{hex} , or the hexagon vector \vec{v}_{hex} and the basic vector \vec{V}_k , $k \in \{1, 2, 3, 4, 5, 6\}$ is the central idea of the overmodulation technique, where:

$$\begin{cases} \vec{V}_1 \text{ and } \vec{V}_4 \text{ can be generated from states } \pm 1, \pm 2, \text{ and } \pm 3 \\ \vec{V}_2 \text{ and } \vec{V}_5 \text{ can be generated from states } \pm 4, \pm 5, \text{ and } \pm 6 \\ \vec{V}_3 \text{ and } \vec{V}_6 \text{ can be generated from states } \pm 7, \pm 8, \text{ and } \pm 9 \end{cases}$$

3.1. Overmodulation mode I: $0.866 < q \leq 0.909$

Both the inscribed circle vector \vec{v}_{\sin} and the hexagon vector \vec{v}_{hex} are used to generate the output voltage vector \vec{v}_o in overmodulation region I:

$$\vec{v}_o = k_f \vec{v}_{\text{hex}} + (1 - k_f) \vec{v}_{\sin} \quad (12)$$

where the parameter k_f is defined as:

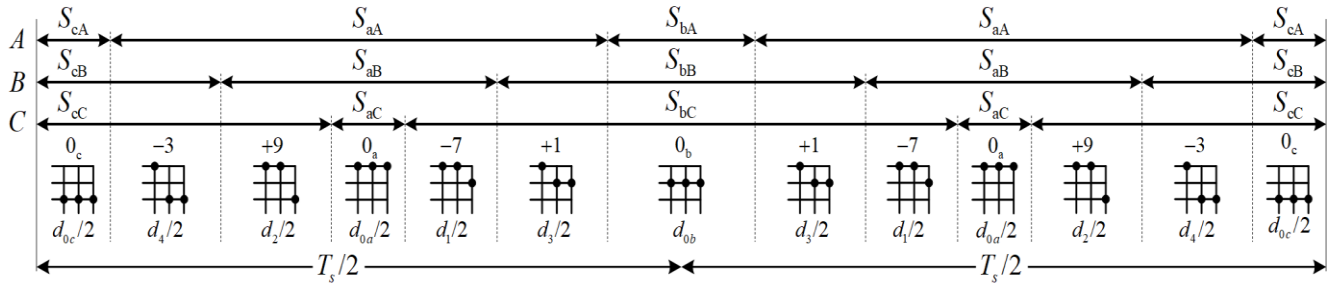
$$k_f = \frac{q - 0.866}{V_{\text{hex}(1)} / V_i - 0.866} = \frac{q - 0.866}{0.909 - 0.866} \quad (13)$$

Here, $V_{\text{hex}(1)} = 0.909V_i$ represents the fundamental amplitude of the hexagon vector \vec{v}_{hex} [4].

To generate the inscribed circle vector \vec{v}_{\sin} , the duty cycles of the active and zero vectors are determined as follows:

Table 2: Selected SCs for every Sector Combination of Input Current and Output Voltage in the Traditional SVM Method

		Input Current Vector Sector																							
		1				2				3				4				5				6			
Output Voltage Vector Sector	1	-7	+9	+1	-3	+9	-8	-3	+2	-8	+7	+2	-1	+7	-9	-1	+3	-9	+8	+3	-2	+8	-7	-2	+1
	2	+4	-6	-7	+9	-6	+5	+9	-8	+5	-4	-8	+7	-4	+6	+7	-9	+6	-5	-9	+8	-5	+4	+8	-7
	3	-1	+3	+4	-6	+3	-2	-6	+5	-2	+1	+5	-4	+1	-3	-4	+6	-3	+2	+6	-5	+2	-1	-5	+4
	4	+7	-9	-1	+3	-9	+8	+3	-2	+8	-7	-2	+1	-7	+9	+1	-3	+9	-8	-3	+2	-8	+7	+2	-1
	5	-4	+6	+7	-9	+6	-5	-9	+8	-5	+4	+8	-7	+4	-6	-7	+9	-6	+5	+9	-8	+5	-4	-8	+7
	6	+1	-3	-4	+6	-3	+2	+6	-5	+2	-1	-5	+4	-1	+3	+4	-6	+3	-2	-6	+5	-2	+1	+5	-4
Duty cycles		d_1	d_2	d_3	d_4	d_1	d_2	d_3	d_4	d_1	d_2	d_3	d_4	d_1	d_2	d_3	d_4	d_1	d_2	d_3	d_4	d_1	d_2	d_3	d_4

**Figure 4:** Switching pattern for the traditional SVM method when the input current and output voltage lie in sector 1.

$$\begin{cases} d_{1,\sin} = d_1 \Big|_{q=\frac{\sqrt{3}}{2} \cos \delta_i} = \sin \tilde{\alpha}_o \sin(\pi/6 - \tilde{\beta}_i) \\ d_{2,\sin} = d_2 \Big|_{q=\frac{\sqrt{3}}{2} \cos \delta_i} = \sin \tilde{\alpha}_o \sin(\pi/6 + \tilde{\beta}_i) \\ d_{3,\sin} = d_3 \Big|_{q=\frac{\sqrt{3}}{2} \cos \delta_i} = \sin(\pi/3 - \tilde{\alpha}_o) \sin(\pi/6 - \tilde{\beta}_i) \\ d_{4,\sin} = d_4 \Big|_{q=\frac{\sqrt{3}}{2} \cos \delta_i} = \sin(\pi/3 - \tilde{\alpha}_o) \sin(\pi/6 + \tilde{\beta}_i) \\ d_{0,\sin} = d_0 \Big|_{q=\frac{\sqrt{3}}{2} \cos \delta_i} = 1 - \cos(\pi/6 - \tilde{\alpha}_o) \cos \tilde{\beta}_i \end{cases} \quad (\text{II})$$

Similarly, the duty cycles for the hexagon vector \vec{v}_{hex} are calculated based on (I) and (7), as $q = \frac{\sqrt{3}}{2} \frac{\cos \delta_i}{\cos(\pi/6 - \tilde{\alpha}_o)}$:

$$\begin{cases} d_{1,\text{hex}} = \frac{\sin \tilde{\alpha}_o \sin(\pi/6 - \tilde{\beta}_i)}{\cos(\pi/6 - \tilde{\alpha}_o)} \\ d_{2,\text{hex}} = \frac{\sin \tilde{\alpha}_o \sin(\pi/6 + \tilde{\beta}_i)}{\cos(\pi/6 - \tilde{\alpha}_o)} \\ d_{3,\text{hex}} = \frac{\sin(\pi/3 - \tilde{\alpha}_o) \sin(\pi/6 - \tilde{\beta}_i)}{\cos(\pi/6 - \tilde{\alpha}_o)} \\ d_{4,\text{hex}} = \frac{\sin(\pi/3 - \tilde{\alpha}_o) \sin(\pi/6 + \tilde{\beta}_i)}{\cos(\pi/6 - \tilde{\alpha}_o)} \\ d_{0,\text{hex}} = 1 - \cos \tilde{\beta}_i \end{cases} \quad (\text{III})$$

Lastly, for overmodulation mode I, the total duty cycles of the active and zero vectors are provided by:

$$\begin{cases} d_1 = k_I d_{1,\text{hex}} + (1 - k_I) d_{1,\sin} \\ d_2 = k_I d_{2,\text{hex}} + (1 - k_I) d_{2,\sin} \\ d_3 = k_I d_{3,\text{hex}} + (1 - k_I) d_{3,\sin} \\ d_4 = k_I d_{4,\text{hex}} + (1 - k_I) d_{4,\sin} \\ d_0 = k_I d_{0,\text{hex}} + (1 - k_I) d_{0,\sin} \end{cases} \quad (\text{IV})$$

3.2. Overmodulation mode II: $0.909 < q \leq 0.955$

Both the basic vector \vec{V}_k , $k \in \{1, 2, 3, 4, 5, 6\}$ and the hexagon vector \vec{v}_{hex} are used to create the output voltage vector in overmodulation region II:

$$\vec{v}_o = k_{II} \vec{V}_k + (1 - k_{II}) \vec{v}_{\text{hex}} \quad (14)$$

where the parameter k_{II} is defined as:

$$k_{II} = \frac{q - 0.909}{V_{k(1)} / V_i - 0.909} = \frac{q - 0.909}{0.955 - 0.909} \quad (15)$$

Here, $V_{k(1)} = 0.955V_i$ represents the fundamental amplitude of the basic vector \vec{V}_k [4].

The duty cycles of the active and zero vectors are calculated as follows to create the basic vector \vec{V}_k :

- For \vec{V}_1 :
$$\begin{cases} d_{1,V_1} = d_1 \Big|_{q=1, \tilde{\alpha}_o=0} = 0 \\ d_{2,V_1} = d_2 \Big|_{q=1, \tilde{\alpha}_o=0} = 0 \\ d_{3,V_1} = d_3 \Big|_{q=1, \tilde{\alpha}_o=0} = \sin(\pi/6 - \tilde{\beta}_i) \\ d_{4,V_1} = d_4 \Big|_{q=1, \tilde{\alpha}_o=0} = \sin(\pi/6 + \tilde{\beta}_i) \\ d_{0,V_1} = d_0 \Big|_{q=1, \tilde{\alpha}_o=0} = 1 - \cos \tilde{\beta}_i \end{cases} \quad (\text{V})$$

- For \vec{V}_2 :

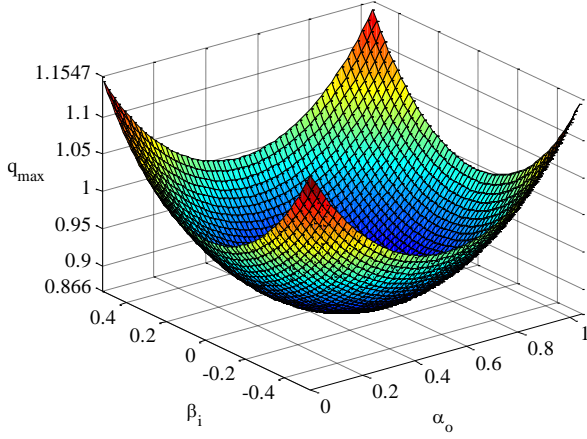


Figure 5: Maximum VTR in relation to $\tilde{\alpha}_o$ and $\tilde{\beta}_i$.

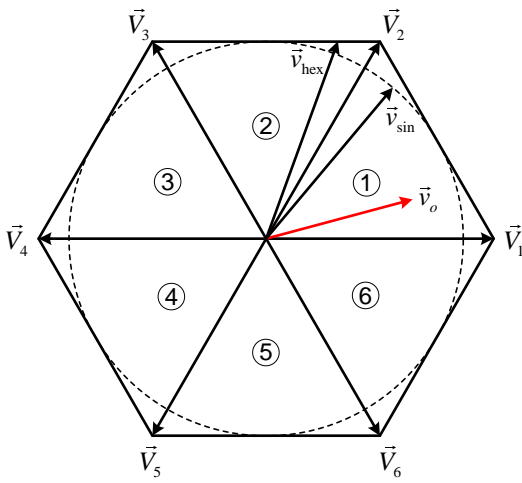


Figure 6: Inscribed circle vector, hexagon vector, and basic vector.

$$\begin{cases} d_{1,V_2} = d_1|_{q=1, \tilde{\alpha}_o = \pi/3} = \sin(\pi/6 - \tilde{\beta}_i) \\ d_{2,V_2} = d_2|_{q=1, \tilde{\alpha}_o = \pi/3} = \sin(\pi/6 + \tilde{\beta}_i) \\ d_{3,V_2} = d_3|_{q=1, \tilde{\alpha}_o = \pi/3} = 0 \\ d_{4,V_2} = d_4|_{q=1, \tilde{\alpha}_o = \pi/3} = 0 \\ d_{0,V_2} = d_0|_{q=1, \tilde{\alpha}_o = \pi/3} = 1 - \cos \tilde{\beta}_i \end{cases} \quad (VI)$$

Lastly, for overmodulation mode II, the total duty cycles of the active and zero vectors are:

$$\begin{cases} \begin{cases} d_1 = k_{II}d_{1,V_1} + (1 - k_{II})d_{1,hex} \\ d_2 = k_{II}d_{2,V_1} + (1 - k_{II})d_{2,hex} \\ d_3 = k_{II}d_{3,V_1} + (1 - k_{II})d_{3,hex} \\ d_4 = k_{II}d_{4,V_1} + (1 - k_{II})d_{4,hex} \\ d_0 = k_{II}d_{0,V_1} + (1 - k_{II})d_{0,hex} \end{cases} & \text{for } 0 \leq \tilde{\alpha}_o < \pi/6 \\ \begin{cases} d_1 = k_{II}d_{1,V_2} + (1 - k_{II})d_{1,hex} \\ d_2 = k_{II}d_{2,V_2} + (1 - k_{II})d_{2,hex} \\ d_3 = k_{II}d_{3,V_2} + (1 - k_{II})d_{3,hex} \\ d_4 = k_{II}d_{4,V_2} + (1 - k_{II})d_{4,hex} \\ d_0 = k_{II}d_{0,V_2} + (1 - k_{II})d_{0,hex} \end{cases} & \text{for } \pi/6 \leq \tilde{\alpha}_o < \pi/3 \end{cases} \quad (VII)$$

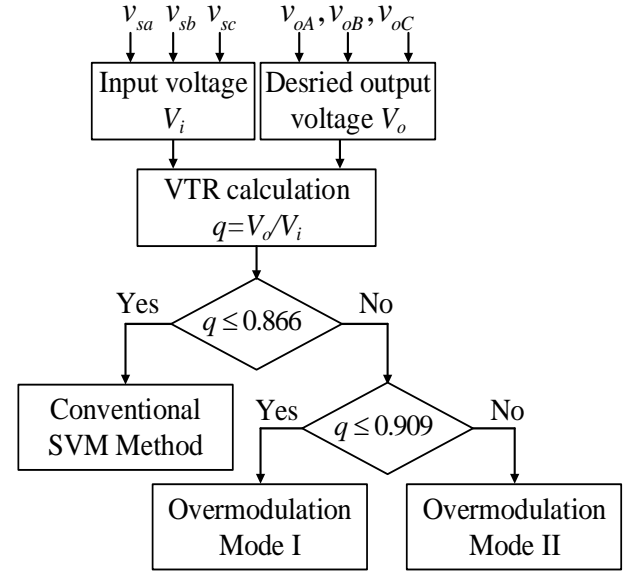


Figure 7: Effective flowchart to achieve full VTR operation.

Table 3: System Parameters

Power supply	Input filter	Output load
$V_s = 100V$	$L_f = 1.4 \text{ mH}$	$R = 20 \Omega$
$f_i = 60 \text{ Hz}$	$C_f = 22 \mu\text{F}$	$L = 10 \text{ mH}$
	$R_d = 20 \Omega$	$f_o = 50 \text{ Hz}$

The efficient flowchart for achieving full VTR operation of the three-phase MCs using the proposed modulation approach is displayed in Figure 7. According to (9), when the VTR is less than 0.866, the traditional SVM approach is appropriate for the use case. In the meantime, as stated in sections 3.1 and 3.2, the proposed overmodulation mode I is chosen for the VTR range of 0.866 to 0.909, and the proposed overmodulation mode II can be employed with the VTR range of 0.909 to 0.955.

4. Simulation Results

To validate the theoretical analysis, simulations were conducted using PSIM software utilizing the system characteristics stated in Table 3. The switching frequency was set to 10kHz, corresponding to a switching period of 100 μ s. The simulation results for the space-vector overmodulation approach in mode I, with a VTR of 0.9 and an output frequency of 50 Hz, are shown in Figure 8. Both the input and output currents are almost sinusoidal, indicating a low degree of harmonic distortion, as seen in Figures 7(a) and 7(b). The output phase voltage waveforms and its Fast Fourier Transform (FFT) analysis are shown in Figures 7(c) and 7(d). At 90V, or 90% of the input voltage amplitude, the fundamental component of the output voltage peaks. The simulation results for mode II of the space-vector overmodulation approach, with a VTR of 0.95 and an output frequency of 50 Hz, are displayed in Figure 9. The input and

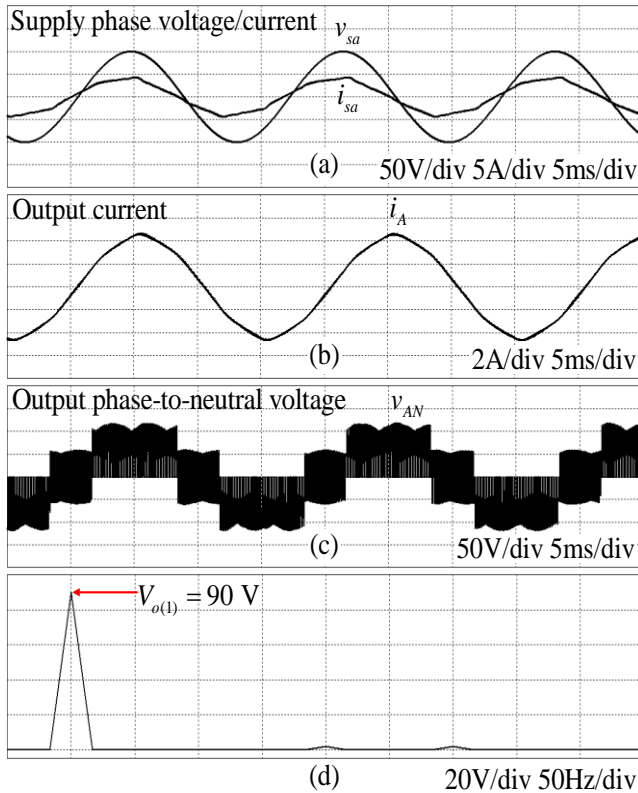


Figure 8: (a) Supply phase voltage and current. (b) Output current. (c) Output phase-to-neutral voltage and its (d) FFT analysis with the direct space-vector overmodulation method mode I at $f_o = 50$ Hz, $q = 0.9$.

output currents are shown in Figures 8(a) and 8(b), where the greater overmodulation range causes observable distortion. The output phase voltage waveforms and the associated FFT analysis are shown in Figures 8(c) and 8(d). The output voltage's basic component peaks at 95V, which corresponds to 95% of the input voltage amplitude. Consequently, the efficiency of the proposed overmodulation technique is confirmed by the simulation results, which support the theoretical investigation.

5. Conclusion

A multimode space-vector overmodulation technique for MCs to improve VTR was presented in this paper. By combining the principles of the hexagon vector with the basic vector or the inscribed circle vector with the hexagon vector, the suggested method increases the VTR. Interestingly, the choice of active and zero vectors is in line with the traditional method, and specific formulas for determining their duty cycles are given. Simulations were used to verify the efficacy of the proposed method and show precise output voltage fundamental components, so validating the theoretical analysis's accuracy.

References

[1] A. Sarajian *et al.*, "Enhanced Modulated Model Predictive Control for Matrix Converters in Overmodulation Zones," in *IEEE Open Journal of Power Electronics*, vol. 6, pp. 66-77, 2025, <https://doi.org/10.1109/OJPEL.2024.3512855>

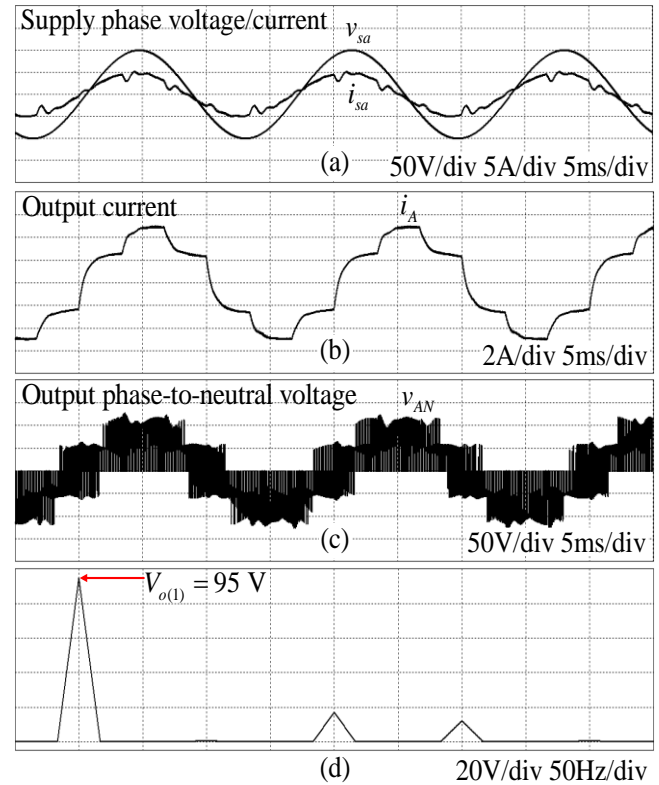


Figure 9: (a) Supply phase voltage and current. (b) Output current. (c) Output phase-to-neutral voltage and its (d) FFT analysis with the direct space-vector overmodulation method mode II at $f_o = 50$ Hz, $q = 0.95$.

- [2] G. Mirzaeva and Y. Liu, "Matrix Converters: Challenges and Solutions," in *IEEE Transactions on Industry Applications*, vol. 59, no. 6, pp. 7919-7928, Nov.-Dec. 2023, <https://doi.org/10.1109/TIA.2023.3299911>.
- [3] Tran, H., Vu, T., & Nguyen, T. (2021). Space-vector modulation for three-phase indirect matrix converters to reduce common-mode voltage. *VNUHCM Journal of Engineering and Technology*, 4(2), 846-860. <https://doi.org/10.32508/stdjet.v4i2.797>
- [4] Y. Xia, X. Zhang, M. Qiao, F. Yu, Y. Wei and P. Zhu, "Research on a New Indirect Space-Vector Overmodulation Strategy in Matrix Converter," in *IEEE Transactions on Industrial Electronics*, vol. 63, no. 2, pp. 1130-1141, Feb. 2016, <https://doi.org/10.1109/TIE.2015.2480382>
- [5] von Jouanne A, Agamloh E, Yokochi A. A Review of Matrix Converters in Motor Drive Applications. *Energies*. 2025; 18(1):164. <https://doi.org/10.3390/en18010164>
- [6] J. Lei, B. Zhou, J. Bian, J. Wei, Y. Zhu, J. Yu, and Y. Yang, "Feedback control strategy to eliminate the input current harmonics of matrix converter under unbalanced input voltages," *IEEE Trans. Power Electron.*, vol. 32, no. 1, pp. 878-888, Jan. 2017. <https://doi.org/10.1109/TPEL.2016.2539398>
- [7] Q. -H. Tran and H. -H. Lee, "An Advanced Modulation Strategy for Three-to-Five-Phase Indirect Matrix Converters to Reduce Common-Mode Voltage with Enhanced Output Performance," in *IEEE Transactions on Industrial Electronics*, vol. 65, no. 7, pp. 5282-5291, July 2018. <https://doi.org/10.1109/TIE.2017.2782242>
- [8] Li, S., Lu, Z., Cao, S. *et al.* 71% Common-mode voltage suppression modulation strategy for indirect matrix converters. *J. Power Electron.* 23, 171-180 (2023). <https://doi.org/10.1007/s43236-022-00531-w>
- [9] Q. -H. Tran, T. D. Nguyen and L. M. Phuong, "Simplified Space-Vector Modulation Strategy for Indirect Matrix Converter With Common-Mode Voltage and Harmonic Distortion Reduction," in *IEEE Access*, vol. 8, pp. 218489-218498, 2020. <https://doi.org/10.1109/ACCESS.2020.3042528>
- [10] B. Shi, B. Zhou, Y. Zhu, X. Qin, J. Lei and N. Han, "Open-Circuit Fault Analysis and Diagnosis for Indirect Matrix Converter," in *IEEE Journal of Emerging and Selected Topics in Power Electronics*, vol. 6, no. 2, pp. 770-781, June 2018. <https://doi.org/10.1109/JESTPE.2017.2772788>.
- [11] X. Li, Y. Sun, J. Zhang, M. Su and S. Huang, "Modulation Methods for Indirect Matrix Converter Extending the Input Reactive Power Range,"

- in *IEEE Transactions on Power Electronics*, vol. 32, no. 6, pp. 4852-4863, June 2017. <https://doi.org/10.1109/TPEL.2016.2599642>
- [12] H. -N. Nguyen and H. -H. Lee, "An Effective SVM Method for Matrix Converters With a Superior Output Performance," in *IEEE Transactions on Industrial Electronics*, vol. 65, no. 9, pp. 6948-6958, Sept. 2018. <https://doi.org/10.1109/TIE.2017.2779438>
- [13] T. Wijekoon, C. Klumpner and P. Wheeler, "Implementation of a hybrid AC/AC direct power converter with unity voltage transfer ratio," *Twenty-First Annual IEEE Applied Power Electronics Conference and Exposition, 2006. APEC '06.*, Dallas, TX, USA, 2006, pp. 7. <https://doi.org/10.1109/APEC.2006.1620735>.
- [14] E. Karaman, M. Farasat and A. M. Trzynadlowski, "A Comparative Study of Series and Cascaded Z-Source Matrix Converters," in *IEEE Transactions on Industrial Electronics*, vol. 61, no. 10, pp. 5164-5173, Oct. 2014. <https://doi.org/10.1109/TIE.2014.2301766>.
- [15] G. Zhang, J. Yang, Y. Sun, M. Su, Q. Zhu and F. Blaabjerg, "A Predictive-Control-Based Over-Modulation Method for Conventional Matrix Converters," in *IEEE Transactions on Power Electronics*, vol. 33, no. 4, pp. 3631-3643, April 2018. <https://doi.org/10.1109/TPEL.2017.2710909>.
- [16] S. Li, C. Xia, Y. Yan and T. Shi, "Space-Vector Overmodulation Strategy for Ultrasparse Matrix Converter Based on the Maximum Output Voltage Vector," in *IEEE Transactions on Power Electronics*, vol. 32, no. 7, pp. 5388-5397, July 2017. <https://doi.org/10.1109/TPEL.2016.2604418>.
- [17] S. Li, W. Chen, Y. Yan, T. Shi and C. Xia, "A Multimode Space Vector Overmodulation Strategy for Ultrasparse Matrix Converter With Improved Fundamental Voltage Transfer Ratio," in *IEEE Transactions on Power Electronics*, vol. 33, no. 8, pp. 6782-6793, Aug. 2018. <https://doi.org/10.1109/TPEL.2017.2752748>
- [18] Bozorgi, A.M., Monfared, M. and Rajabi Mashhadi, H. (2014), Two simple overmodulation algorithms for space vector modulated three-phase to three-phase matrix converter. *IET Power Electronics*, 7: 1915-1924. <https://doi.org/10.1049/iet-pel.2013.0740>